

Research Paper

Aspects of the Aligned Magnetic Field Past a Stratified Inclined Sheet with Nonlinear Convection and Variable Thermal Conductivity

Muhammad BILAL¹*, Saba INAM²), Shamsa KANWAL²),
Muzma NAZEER¹)

¹) *The University of Lahore Gujrat Campus*
Gujrat, Pakistan

*Corresponding Author e-mail: m.bilal@math.uol.edu.pk

²) *Fatima Jinnah Women University*
Rawalpindi, Pakistan

An analytical study of a two-dimensional boundary layer flow of an upper-convected Maxwell fluid is examined. In addition, an aligned magnetic field over the inclined shrinking/stretching stratified sheet in a non-Darcian porous medium is considered. The heat transfer effects are employed through nonlinear convection and variable thermal conductivity. The associated higher-order nonlinear equations are transformed to ordinary first-order differential equations by using similarity transformation. The resulting ordinary first-order differential equations are then solved numerically by the shooting method. This paper aims to investigate the special effects of parameters on velocity and temperature profiles. The results are also discussed, graphically and numerically for the skin friction and Nusselt number.

Key words: inclined sheet; stratification; nonlinear convection; Darcy-Forchheimer flow; aligned magnetic field.

NOTATIONS

- (u, v) – velocity components [m/s],
- (x, y) – coordinate axis [m],
- (ω_1, ω_2) – initial guesses,
- a, b – dimensional constant,
- a_1, d_1 – dimensional constant [s^{-1}],
- B_0 – magnetic field strength [$kg/(s^2 \cdot A)$],
- C_b – drag coefficient,

C_f	-	skin friction coefficient,
c_p	-	specific heat [J/(kg·K)],
f'	-	dimensionless velocity,
F	-	variable inertia coefficient,
F_r	-	local inertia coefficient,
g	-	gravitational acceleration [m/s ²],
Gr_x	-	Grashof number,
K	-	porous medium permeability,
k	-	variable thermal conductivity [W/(m·K)],
k_∞	-	thermal conductivity coefficient,
M	-	magnetic parameter,
Nu_x	-	local Nusselt number,
Pr	-	Prandtl number,
q_w	-	surface heat flux [W/(m·K)],
Re_x	-	local Reynolds number,
S	-	suction/injection parameter,
S_1	-	thermal stratification variable,
T	-	fluid temperature [K],
T_0	-	reference temperature [K],
T_∞	-	ambient liquid temperature [K],
T_f	-	heated liquid temperature [K],
u_w	-	stretching velocity [m/s],
v_0	-	mass flux velocity [m/s],
α	-	angle of inclination,
α_t	-	thermal conductivity parameter,
β	-	dimensionless Maxwell parameter,
β_1	-	linear thermal coefficient [K ⁻¹],
β_2	-	nonlinear expansion coefficient [K ⁻¹],
β_t	-	nonlinear thermal variable,
γ	-	aligned magnetic angle,
δ	-	mixed convection variable,
ϵ	-	stretching/shrinking parameter,
η	-	similarity variable,
θ	-	dimensionless temperature,
λ	-	relaxation time parameter [s],
λ_1	-	porosity parameter,
μ	-	dynamic viscosity [kg/(m·s)],
ν	-	kinematic viscosity [m ² /s],
ρ	-	fluid density [kg/m ³],
σ	-	electrical conductivity [S/m],
τ_w	-	shear stress,
Ψ	-	stream function.

1. INTRODUCTION

Non-Newtonian fluids have attracted a significant attention of scientists due to their wide applications in different technologies and engineering. Because of the fast development of annealing and thinning of copper wires, aerodynamic liquid film condensation process, and emission of plastic films, etc., [1], it is indispensable to investigate different non-Newtonian models. Several studies present concise research related to different surfaces and geometries promoting its applications to numerous industries. SAKIADIS [2] was the first to study the boundary layer flow with a constant speed past a persistent solid panel. Since then, numerous research studies have been carried out for different types of non-Newtonian fluids flowing over the stretched surface [3–6]. All the characteristics of these types of fluid models cannot be constituted by a single equation. Therefore, researchers proposed various non-Newtonian fluid structures with different geometries [7–9]. These structures are classified as differential, rate, and integral types. Maxwell model is one of the rate type fluid with relaxation time phenomenon. Consequently, an upper-convected Maxwell fluid model is significant for application purposes [10]. The heat transfer combined with boundary layer flow due to the stretching sheet for the upper-convected Maxwell fluid has been studied by many scientists.

The phenomenon of the transfer of internal energy from one substance to another is known as heat transfer and it attracts the attention of many mathematicians, researchers, engineers, and physicists. Due to the impact of heat transfer in various substances and boundary layer flows over a stretching sheet, there are extensive applications in biology, engineering, and industry for example fermentation process, metal extrusion, paper production, bubble absorption, etc. [11–21]. Conduction, convection, and radiation are the three ways of heat transfer. The transfer of heat through physical interaction, fluid motion, and radiation is known as conduction, convection, and radiation respectively. Generally, convection means heat transfer between some types of fluid and a surface (fixed or moving), and forced convection is caused by an external force for transferring heat between two substances. The deliberation of this attribute is necessary, particularly in the field of geophysical and astrophysical branches. Most of the available literature comprises linear convection, but in fact nonlinear convection is more appropriate for the study of heat transfer.

Porous mediums can be found in almost all fields of science and engineering, such as mechanical engineering, biology, geophysics, chemical and petroleum engineering, and more. The study of heat transfer in porous medium plays a vital role in transportation phenomena. Due to the natural properties of pseudo-continuity, thermal transport in porous medium demonstrates fascinating behavior generally not present in the non-porous medium. So far, a vast literature has

been devoted to heat transfer in porous media. However, with the emergence of innovative knowledge and interdisciplinary combination, heat transfer in porous media exhibits exclusive trends in current years, such as heat transfer in nanoporous medium, coupled flow, and reactive flow through porous medium [22]. The fluid models involving porous medium within high-velocity systems are a challenging field for researchers. Recently, non-Darcy effects on natural convection in the porous medium have greatly impacted the experiments carried out with several blends of solids and fluids covering widespread governing parameters. These experiments indicate that the experimental records for systems do not agree with the predictions of the Darcy flow model. Generally, there are two classes of non-Darcian flows: high-velocity and low-velocity non-Darcian flow. Several nonlinear relations were suggested for the high-velocity non-Darcian flow, for example, the quadratic relationship by FORCHHEIMER [23] and the power function by IZBASH [24]. The investigations of non-Darcian flow in porous media are carried out these days, for example, see [25–27].

The advantageous magnetic field effects on the boundary layer make the investigation of magnetohydrodynamic (MHD) flow very interesting for researchers. The MHD flow with the uniform magnetic field over a stretching surface was studied by PAVLOV [28] and an incompressible viscous fluid flow over a stretching sheet having MHD flow was investigated by ANDERSSON [29]. The study involving the MHD flow of micropolar fluid through a non-Darcy porous medium with Soret effects and thermal reaction is examined by MABOOD *et al.* [30]. In the research work of KHAN *et al.* [31, 33] and KUMAR *et al.* [32], an investigation regarding heat transfer along with source/sink and chemical reaction was carried out through the expanding sheet. A study of a chemical reaction within MHD Maxwell fluid together with heat flux was carried out by RAMZAN *et al.* [34]. The analysis of a chemically reactive magneto-ferrofluid over a sheet with Darcy and non-Darcy porous media was presented by MAJEED *et al.* [35, 36]. The effect of related magnetic fields over a vertical stretching layer was addressed by RAJU *et al.* [37]. They showed that an increase in the aligned angle improves the temperature profile of the fluid and decreases the velocity.

The present study is inspired by the above-cited investigations and their applications to different areas. The main goal of this work is to study the regime of Maxwell fluid. More precisely, this paper deals with the analysis of nonlinear mixed convective flow over the non-Darcian porous media in an aligned magnetic field. Further, the stratified inclined shrinking/stretching panel is used along with variable thermal conductivity. The equations present this phenomenon modeled as coupled nonlinear differential boundary value problem and solved by the nonlinear shooting method. For solving problem arising from nonlinear fluid models, the shooting method has been used effectively in the literature. In Sec. 4,

a comprehensive discussion of the model under consideration along with obtained parameters and graphical results are given.

2. MATHEMATICAL FORMULATION

A non-Newtonian upper-convected Maxwell (UCM) fluid flowing over the two-dimensional inclined stretching/shrinking stratified sheet is considered. The angle of inclination is α while the speed of expansion of the sheet along the x -axis is $u_w(x) = ax$. Further, the magnetic field B_0 is also applied through an angle γ from the y -axis as shown in Fig. 1. Due to stratification, the temperature is linearly dependent on x -direction length, i.e., on the surface is $T_f = T_0 + a_1x$ and far away it is $T_\infty = T_0 + d_1x$. Because of the motion of electrically conducting fluid, the induced magnetic field is ignored. The flow is examined through the modified Darcian porous medium. Nonlinear convection and thermal conductivity are equally used to explore the heat transfer rate through porous media. The Cauchy stress tensor for the Maxwell fluid model is given by

$$(2.1) \quad \mathbf{T} = -p\mathbf{I} + \mathbf{S},$$

where \mathbf{S} is an extra tensor, which is defined for the Maxwell fluid as

$$(2.2) \quad \mathbf{S} + \lambda \frac{D\mathbf{S}}{Dt} = \mu \mathbf{A}_1.$$

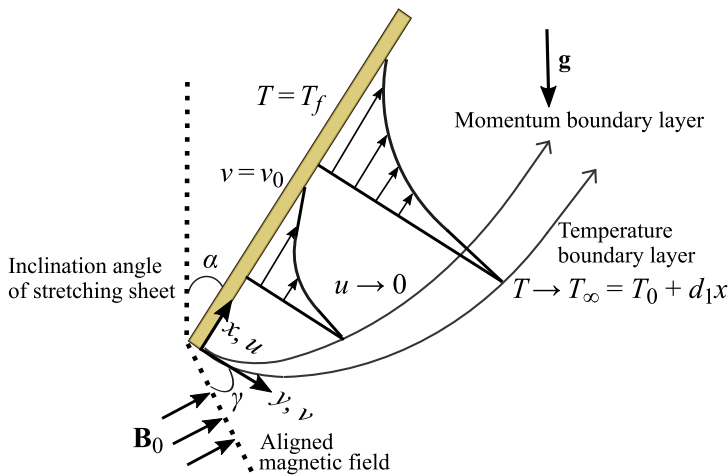


FIG. 1. Geometry for the flow under discussion.

Here, λ , μ , $\frac{D}{Dt}$ and \mathbf{A}_1 are relaxation time, dynamics viscosity, convective derivative and first Rivlin-Ericksen tensor, respectively. The latter two are defined as

$$(2.3) \quad \frac{D\mathbf{S}}{Dt} = \frac{d\mathbf{S}}{dt} - \mathbf{L}\mathbf{S} - \mathbf{S}\mathbf{L}^*,$$

$$(2.4) \quad \mathbf{A}_1 = \nabla\mathbf{V} + (\nabla\mathbf{V})^*,$$

where $*$ denotes the transposition of the tensor and \mathbf{L} is the velocity gradient.

The governing equations of momentum and heat conduction using boundary layer approximation are [38, 39]:

$$(2.5) \quad \frac{\partial u}{\partial x} + \frac{\partial v}{\partial y} = 0,$$

$$(2.6) \quad u \frac{\partial u}{\partial x} + v \frac{\partial u}{\partial y} + \lambda \left(v^2 \frac{\partial^2 u}{\partial y^2} + u^2 \frac{\partial^2 u}{\partial x^2} + 2uv \frac{\partial^2 u}{\partial x \partial y} \right) \\ = \nu \frac{\partial^2 u}{\partial y^2} - \frac{\sigma B_0^2}{\rho} \sin^2(\gamma) \left(u + \lambda v \frac{\partial u}{\partial y} \right) \\ + g(\beta_1 + \beta_2(T - T_\infty))(T - T_\infty) \cos(\alpha) - \left(\frac{\nu}{K} - Fu \right) u,$$

$$(2.7) \quad u \frac{\partial T}{\partial x} + v \frac{\partial T}{\partial y} = \frac{1}{\rho c_p} \frac{\partial}{\partial y} \left(k \frac{\partial T}{\partial y} \right),$$

here, the velocity components (u, v) are along the (x, y) -axis, the (β_1, β_2) are the linear and nonlinear thermal expansion, g is gravitational acceleration, K is permeability of porous medium, coefficient of inertia is $F = C_b/\sqrt{K}$ with C_b being drag coefficient, and the temperature is denoted by T . In the temperature Eq. (2.7), the Fourier law is used defined as

$$(2.8) \quad \mathbf{q} = -k\nabla T,$$

where \mathbf{q} is the local heat flux density, ∇T is a temperature gradient and k is the thermal conductivity taken as variable and defined as [40]

$$(2.9) \quad k = k_\infty \left(1 + \alpha_t \left(\frac{T - T_\infty}{T_f - T_0} \right) \right)$$

with the thermal conductivity parameter α_t defined as

$$(2.10) \quad \alpha_t = \frac{(k - k_\infty)}{k_\infty}.$$

The velocity and temperature of the fluid at surface and far away is described by the following conditions:

$$(2.11) \quad \begin{aligned} \text{at } y = 0, \quad v = v_0, \quad u = \epsilon u_w, \quad T = T_f = T_0 + a_1 x, \\ \text{as } y \rightarrow \infty, \quad T \rightarrow T_\infty = T_0 + d_1 x, \quad u \rightarrow 0, \end{aligned}$$

where v_0 is the mass flux velocity, T_0 is the reference temperature, ϵ is the stretching ($\epsilon > 0$)/shrinking ($\epsilon < 0$) parameter, T_f is the heat liquid temperature, and d_1 and a_1 are dimensional constants. For the similarity solutions, we define the following similarity variables:

$$(2.12) \quad \begin{aligned} \Psi &= \sqrt{v x u_w(x)} f(\eta) = \sqrt{c v} x f(\eta), \\ \eta &= \sqrt{\frac{u_w(x)}{v x}} y = \left(\frac{c}{v}\right)^{1/2} y, \\ \theta(\eta) &= \frac{T - T_\infty}{T_f - T_0}, \end{aligned}$$

where $u = \partial\Psi/\partial y$, $v = -\partial\Psi/\partial x$, and η is the similarity variable. The obtained coupled ordinary differential equations are

$$(2.13) \quad \begin{aligned} f''' - f'^2 + f f'' - \beta (f^2 f''' - 2 f f' f'') - (f' - \beta f f'') M \sin^2(\gamma) \\ + \delta \cos(\alpha) \theta (1 + \beta_t \theta) - F_r f'^2 - \lambda_1 f' = 0, \end{aligned}$$

$$(2.14) \quad (1 + \alpha_t \theta) \theta'' + \alpha_t \theta'^2 + \text{Pr} f \theta' - \text{Pr} (\theta + S_1) f' = 0,$$

and the boundary conditions are as follows:

$$(2.15) \quad \begin{aligned} \text{at } \eta = 0, \quad f(0) = S, \quad f'(0) = \epsilon, \quad \theta(0) = 1 - S_1, \\ \text{as } \eta \rightarrow \infty, \quad \theta(\eta) \rightarrow 0, \quad f'(\eta) \rightarrow 0, \end{aligned}$$

where primes designate the differentiation w.r.t. η , Pr , δ , β , β_t , F_r , M , λ_1 , the Prandtl number, the mixed convection parameter, the Maxwell fluid parameter, nonlinear convection parameter, local inertia coefficient, magnetic parameter, porosity parameter, respectively. Further, S_1 and S are the thermal stratification parameters, the suction/injection parameter with $S < 0$ for injection and $S > 0$ for suction, and these are characterized as

$$\begin{aligned} \lambda_1 &= \frac{\nu}{K a}, & \beta_t &= \frac{\beta_2 (T_f - T_0)}{\beta_1}, & \delta &= \frac{\text{Gr}_x}{\text{Re}_x^2}, & F_r &= \frac{C_b}{\sqrt{K}} x, \\ \text{Pr} &= \frac{\mu c_p}{k}, & \text{Re}_x &= \frac{x u_w}{\nu}, & \text{Gr}_x &= g \beta_1 \frac{(T_f - T_0) x^3}{\nu^2}, & u_w &= a x, \\ M &= \sigma \frac{B_0^2}{\rho a}, & \beta &= \lambda a, & S_1 &= \frac{d_1}{a_1}, & \mu &= \rho \nu. \end{aligned}$$

For the operative purpose, the skin friction coefficient C_f and the local Nusselt number Nu_x can be solved by the functions $f(\eta)$ and $\theta(\eta)$ respectively as

$$(2.16) \quad C_f = \frac{\tau_w}{\rho u_w^2(x)/2}, \quad Nu_x = \frac{xq_w}{k(T_w - T_\infty)},$$

whereas $q_w = -k(\partial T/\partial y)_{y=0}$ is the heat flux and $\tau_w = \mu(\partial u/\partial y)_{y=0}$ is the shear stress at the surface. In dimensionless form, we obtain

$$(2.17) \quad Nu_x/Re_x^{1/2} = -\theta'(0), \quad \frac{1}{2}C_f Re_x^{1/2} = f''(0).$$

3. SOLUTION METHODOLOGY

Since these ODEs are nonlinear and coupled equations, the boundary value problems (2.13) and (2.14) are difficult to solve analytically. As a result, the shooting approach has been considered for numerical solutions. The Newton’s method and fourth-order Runge-Kutta method are essential components of the shooting method for solving nonlinear first-order differential equations. To obtain the first-order ordinary differential equations, we use the following notations:

$$(3.1) \quad f = m_1, \quad f' = m'_1 = m_2, \quad f'' = m'_2 = m_3, \quad \theta = m_4, \quad \theta' = m'_4 = m_5.$$

By using the notations (3.1), we get the following IVP:

$$(3.2) \quad \begin{aligned} m'_1 &= m_2, & m'_2 &= m_3, & m'_3 &= \frac{a^*}{(1 - \beta m_1^2)}, \\ m'_4 &= m_5, & m'_5 &= \frac{(m_2 m_4 - m_1 m_5 + m_2 S_1) \text{Pr} - \alpha_t m_4^2}{1 + \alpha_t m_4}, \end{aligned}$$

where

$$\begin{aligned} a^* &= -2\beta m_1 m_2 m_3 - m_1 y_3 + M \sin^2(\gamma) [m_2 - \beta m_1 m_3] \\ &\quad + \lambda_1 m_2 - \delta m_4 \cos(\alpha) (1 + \beta_t m_4) + (1 + F_r) m_2^2 \end{aligned}$$

and the essential initial conditions (2.15) takes the following form as

$$(3.3) \quad \begin{aligned} m_1(0) &= S, & m_2(0) &= \epsilon, & m_3(0) &= \omega_1, \\ m_4(0) &= 1 - S_1, & m_5(0) &= \omega_2, \end{aligned}$$

where ω_1 and ω_2 are our first estimates. To numerically achieve the desired results of the aforementioned scheme, we replaced the domain $[0, \infty)$ with the bounded domain $[0, \eta_\infty]$, where η_∞ is a relevant finite positive real number. It is

chosen in such a way that after its basic value, which is normally between [5, 7], the collected findings have not been altered in any way. In (3.3), the missing initial conditions ω_1 and ω_2 are to be selected in percent case so that

$$m_2(\eta_\infty, \omega_1, \omega_2) = 0, \quad m_4(\eta_\infty, \omega_1, \omega_2) = 0.$$

The Newton scheme modifies certain calculations. The algorithmic pattern is repeated until the following condition is met:

$$\max\{|m_2(\eta_\infty, \omega_{1n}, \omega_{2n})|, m_4(\zeta_\infty, \omega_{1n}, \omega_{2n})\} < \chi$$

wherein the tolerance is $\chi > 0$. In this article, $\chi = 10^{-5}$ is fixed for all computations.

4. RESULTS AND DISCUSSIONS

The governing Eqs (2.13) and (2.14) are nonlinear with associated boundary conditions (2.15). These equations have been solved using RK-4 based shooting criteria. The results and graphs depicting the numerical solution and analysis are discussed in this section. The skin friction coefficient with the stretching case and the shrinking case are computed and shown in Tables 1 and 2, respectively. The effect of α_t , λ_1 , γ , ϵ , δ , F_r , β_t , S , S_1 , Pr , M , and β on the temperature and

Table 1. Analogy with earlier work for the numerical calculated Skin friction when $\epsilon = 1.0$, $\alpha_t = 0$, $S = 0$, $M = 0$, $Pr = 1$ (stretching case).

β	$f''(0)$			
	ABEL <i>et al.</i> [41]	WAINI <i>et al.</i> [42]	BILAL and NAZEER [44]	Present
0	-0.999962	-1.00000005	-1.0000000	-1.0000000
0.2	-1.051948	-1.05188989	-1.0518899	-1.0518899
0.4	-1.101850	-1.10190327	-1.1019044	-1.1019044
0.6	-1.150163	-1.15013734	-1.1501382	-1.1501382
0.8	-1.196692	-1.19671125	-1.1967134	-1.1967134
1.2	-1.285257	-1.28536326	-1.2863640	-1.2863640

Table 2. Analogy with earlier work for the numerical calculated Skin friction when $\epsilon = -1.0$, $\alpha_t = 0$, $S = 0$, $M = 0$, $Pr = 1$ (shrinking case).

S	$f''(0)$			
	BHATTACHARYYA [43]	WAINI <i>et al.</i> [42]	BILAL and NAZEER [44]	Present
2	2.414300	2.41421357	2.41421369	2.41421369
3	3.302750	3.30277563	3.30277621	3.30277621
4	4.236099	4.23606797	4.23606814	4.23606814

velocity profile is graphically described. The graphs are drawn for the following specific values: $-1.0 \leq \epsilon \leq 1.0$, $\pi/6 \leq \alpha \leq \pi/2$, $2.0 \leq S \leq 2.6$, $0.1 \leq \delta \leq 0.7$, $0.1 \leq S_1 \leq 0.7$, $0.1 \leq F_r \leq 1.0$, $0.1 \leq \lambda \leq 1.0$, $0.0 \leq M \leq 3.0$, $0.1 \leq \beta_t \leq 1.5$, $\pi/6 \leq \gamma \leq \pi/2$, $0.6 \leq Pr \leq 1.2$, $0 \leq \beta \leq 0.15$.

Figure 2 shows the influence of aligned angle γ for the case of stretching $\epsilon = 1$ on the velocity profile. We note that the velocity of fluid decreases with the increase of γ . The reason behind this phenomenon is that an opposite force to the flow is produced due to an increase in the magnetic field with an increment in the angle γ . This force is known as the Lorentz force which reduces the momentum boundary layer solidity. With the inclination of the stretching sheet (α), it is observed in Fig. 3 that the velocity of the fluid is decreased. Higher the

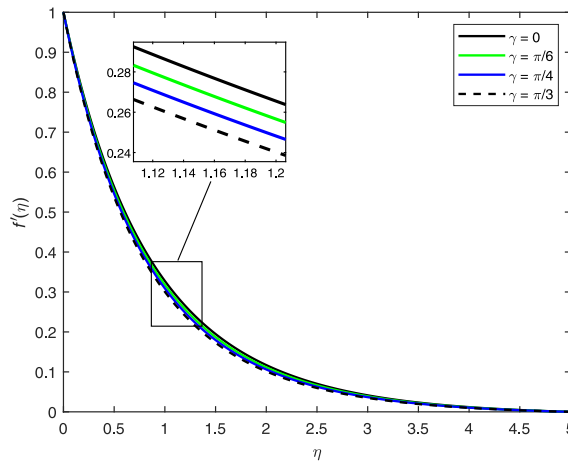


FIG. 2. Impact of magnetic field inclination angle γ on the velocity profile.

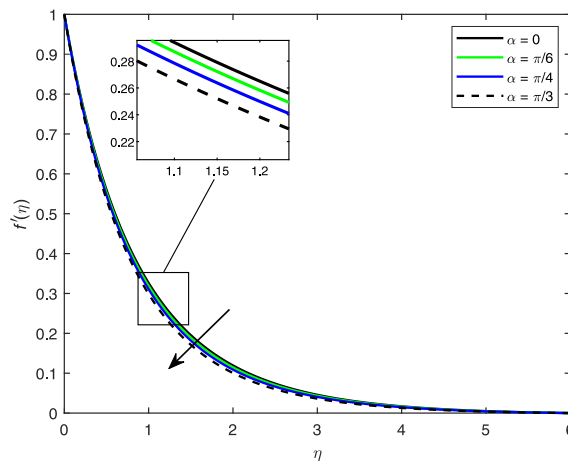


FIG. 3. Impact of wall inclination angle α on the velocity profile.

inclination angle, lower the speed of the fluid; however, this reduction is small. Figure 4 displays the impact of the Maxwell parameter on the velocity profile for the stretching sheet. With the rise of the Maxwell parameter, the velocity profile decreases. $\beta = 0$ corresponds to the Newtonian fluid and the increasing value of β complies with non-Newtonian fluid. Because of the high viscosity in the upper-convected Maxwell fluid, the velocity profile goes down. The graphical representation of the effect of mixed convection parameter δ on the velocity profile is given in Fig. 5, which shows that the significant differences of δ give considerable velocity change. There is an increase in the velocity profile corresponding to the higher linear convection parameter δ . The impact of stretching and shrinking

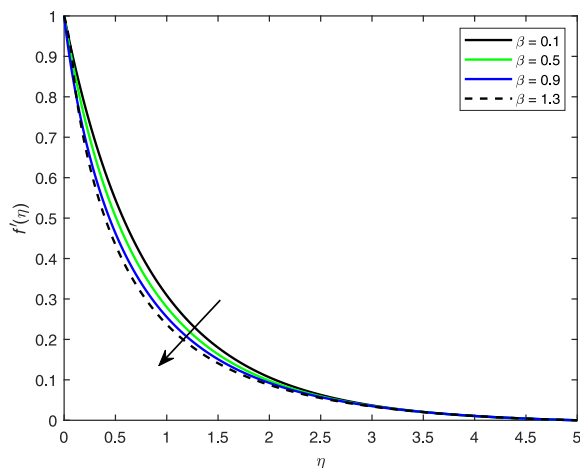


FIG. 4. Impact of the Maxwell fluid parameter β on the velocity profile.

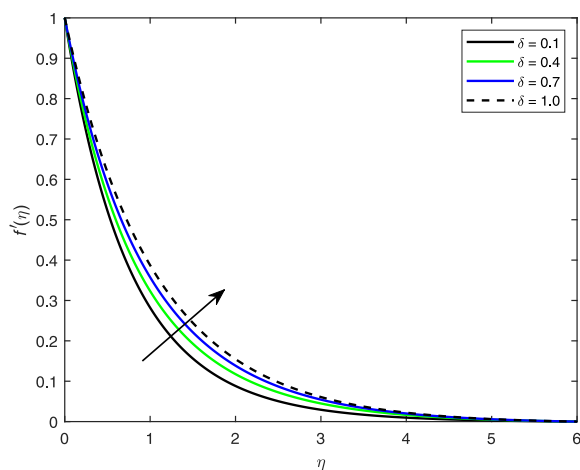


FIG. 5. Impact of mixed convection parameter δ on the velocity profile.

parameter ϵ on the velocity profile is exhibited in Figs 6 and 7, respectively. The positive values of ϵ indicate the stretching case, whereas the negative ϵ shows the shrinking one. It is noted that near the sheet, the velocity increases but away from the sheet it reduces. Opposite action is observed for the shrinking case, as near the plate the velocity dramatically declines, and far away from the sheet, it progresses. Figure 8 describes the behavior of $f'(\eta)$ for numerous values of local inertia coefficient F_r . The enhancement of medium porosity is indicated by the large values of local inertia coefficient, which reduces fluid speed and thickness of boundary layer. With the higher F_r , the size of the pores increases, which ultimately reduces the speed. The influence of porosity parameter λ_1 against the

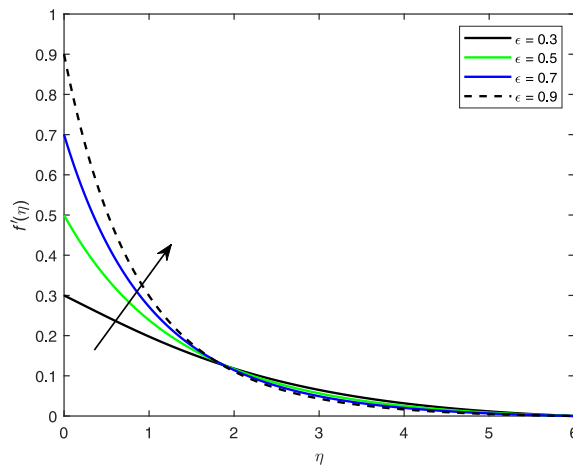


FIG. 6. Impact of stretching parameter ϵ on the velocity profile.

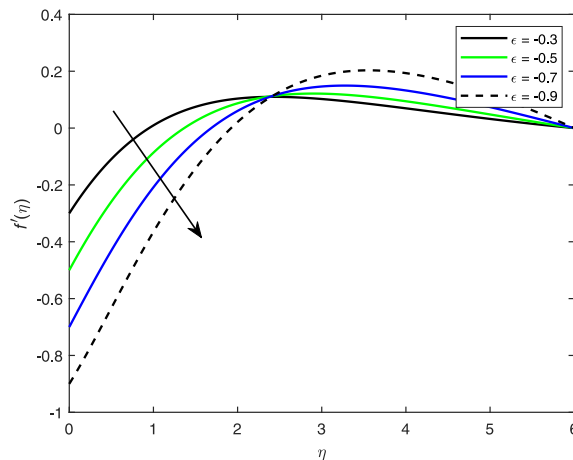


FIG. 7. Impact of shrinking parameter ϵ on the velocity profile.

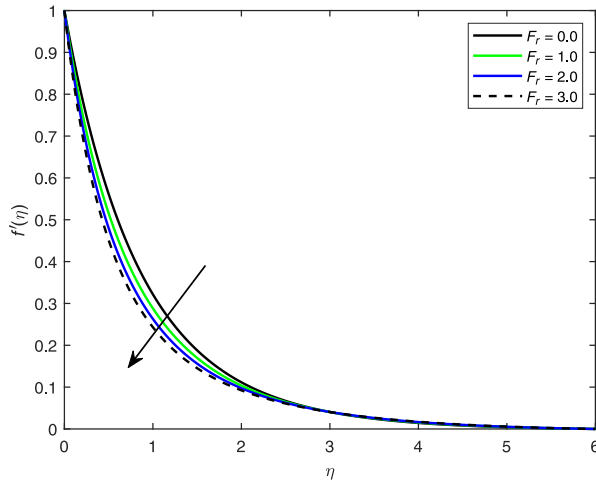


FIG. 8. Impact of local inertia coefficient F_r on the velocity velocity.

velocity f' is reflected in Fig. 9. Quite similar behavior is noted, as observed in the case of inertia coefficient F_r . The porosity parameter is inversely related to the speed of the fluid. The impact of escalating magnetic parameter M on the velocity profile is shown in Fig. 10. Because of the significant Lorentz forces, a conflicting force is produced in the direction of the flow, which resists the motion of the fluid. In Fig. 11, the velocity profile is drawn against the suction parameter S . Due to suction, the speed of the fluid is disturbed and as a result, it is reduced.

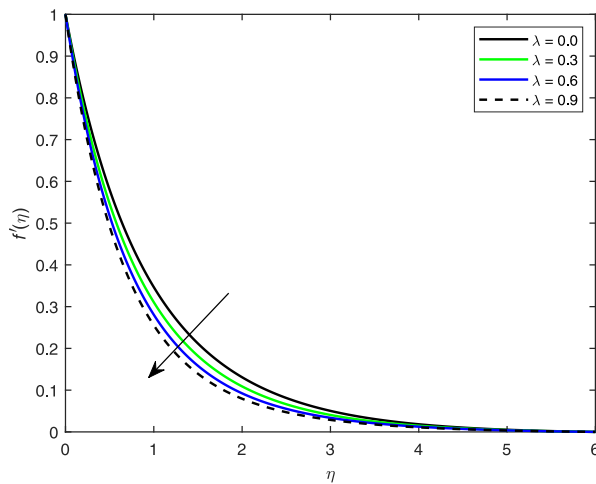
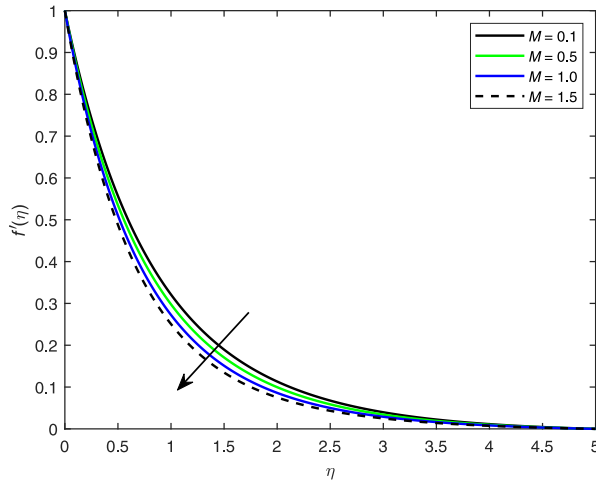
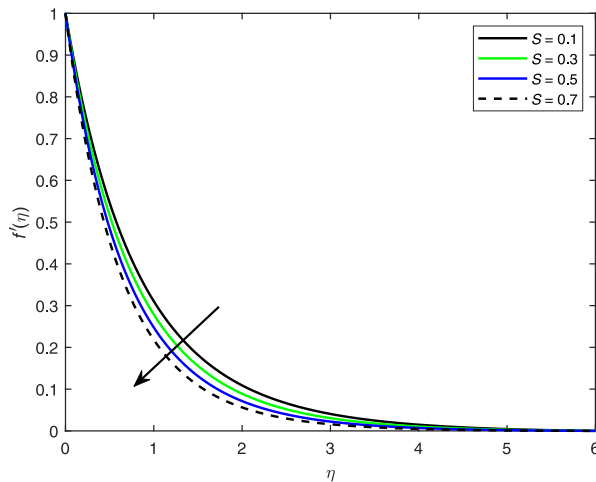
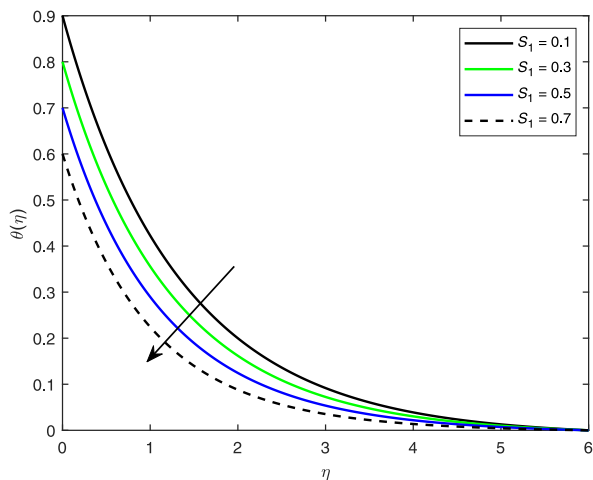
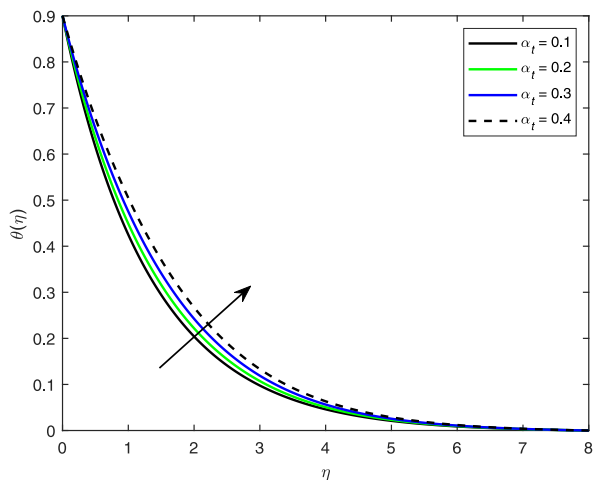


FIG. 9. Impact of time relaxation parameter λ on the velocity profile.

FIG. 10. Impact of magnetic parameter M on the velocity profile.FIG. 11. Impact of suction parameter S on the velocity profile.

It is clear from Fig. 12 that the temperature difference between surface and the ambient decreases with the increase in the thermal stratification parameter S_1 . Physically, the increasing values of S_1 indicate that there is a small difference between the ambient and the surface temperature. This small difference causes a thinner boundary layer thickness and a reduction in temperature. As we have considered a variable thermal conductivity and this conductivity linearly depends on the temperature, with the mounting thermal conductivity parameter α_t , it is observed in Fig. 13 that temperature increases. The effect of

FIG. 12. Impact of thermal stratification S_1 on the velocity profile.FIG. 13. Impact of thermal conductivity parameter α_t on the temperature profile.

behavior of the Prandtl number Pr on the thermal profile is shown in Fig. 14. The temperature $\theta(\eta)$ and associated thermal layer thickness decrease for the larger value of the Prandtl number. The reduction in diffusivity of fluid is due to the large value of the Prandtl number which has an inverse relationship with the thermal diffusivity. This reduction yields a decrease in the temperature profile. Next, Fig. 15 is drawn for the numerically decreasing values of shrinking sheet ϵ against the temperature profile. It is observed in this figure that for the shrinking case, the thermal boundary layer thickness reduces, which ultimately decreases the temperature profile.

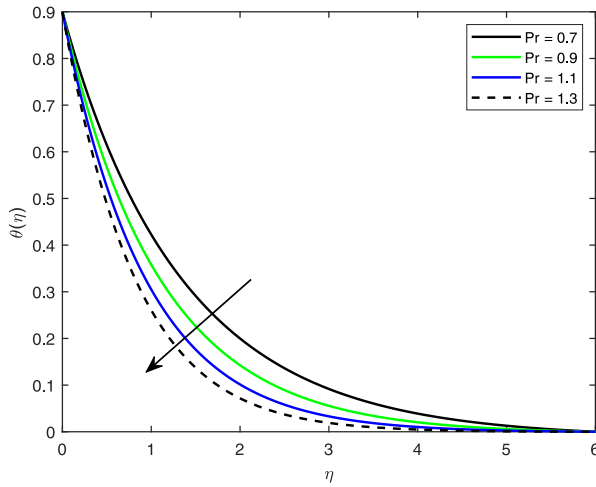


FIG. 14. Impact of Prandtl number Pr on the temperature profile.

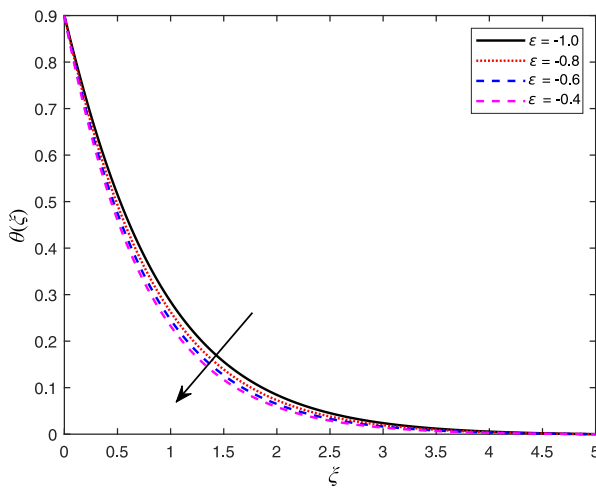


FIG. 15. Impact of stretching parameter ϵ on the temperature profile.

To study the impact of different parameters on the Nusselt number, Figs 16 and 17 are presented. In these graphs, it is observed that higher magnetic parameters create more resistive force during the flow, which enhances the temperature of the fluid. So, the rate of the heat transfer on the surface goes down. Similarly, the Maxwell fluid parameter is also responsible for the decrease of the Nusselt number. In Fig. 17, the stratification parameter S_1 has an inverse relationship with the heat transfer rate $-\theta'(0)$. The higher the stratification parameter the lower the Nusselt number. The Prandtl number is inversely related to thermal

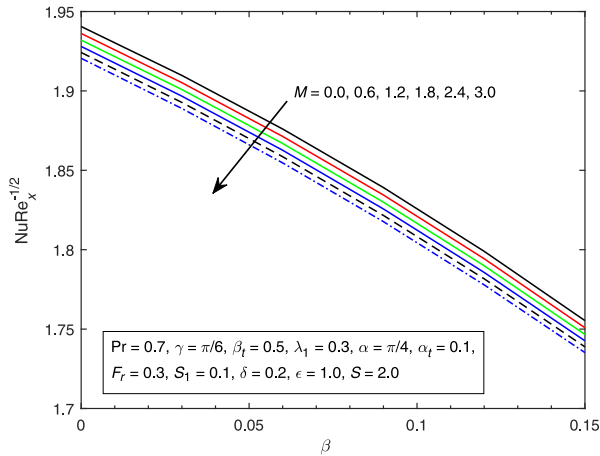


FIG. 16. Impact of magnetic parameter M and Maxwell fluid parameter β on the Nusselt number.

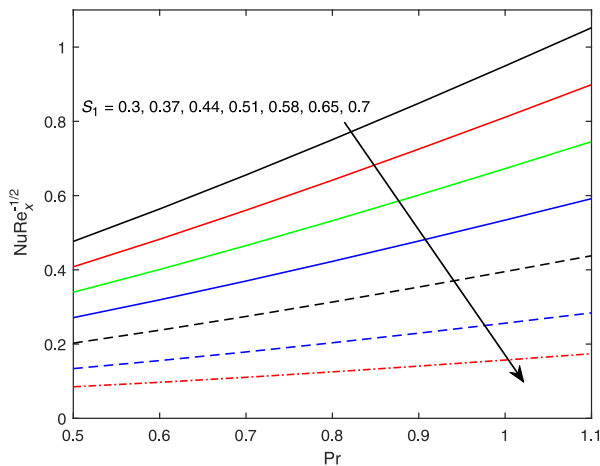


FIG. 17. Impact of Prandtl number Pr and thermal stratification parameter S_1 on the Nusselt number.

diffusivity. A higher Prandtl number can reduce the temperature of the fluid, which resultantly increases the rate of heat transfer on the surface.

The numerically calculated values of the Nusselt number (rate of heat transfer on the surface) and local coefficient of skin friction (retarding acceleration over the stretching sheet) for the emerging parameters are shown in Table 3. The influence of stretching ratio parameter, porosity parameter, inertia coefficient, thermal conductivity parameter, nonlinear thermal convection, mix convection linear parameter, and suction parameter are checked. In this table, it is noted

Table 3. Calculated skin friction and Nusselt number when $\beta = 0.1, M = 0.3, \gamma = \alpha = \pi/4, Pr = 0.7, S_1 = 0.1, \eta = 8.0.$

ϵ	λ_1	β_t	F_r	δ	S	α_t	$-f''(0)$	$-\theta'(0)$
1.0	0.3	0.5	03	0.3	0.1	0.1	1.25731524	0.697815776
0.5							0.38119562	0.508230496
0.6							0.53584036	0.550079499
0.7							0.70066224	0.589762801
	0.4						1.29758484	0.688809432
	0.5						1.33676550	0.680123108
	0.6						1.374937076	0.671736403
		0.2					1.275781175	0.694599086
		0.3					1.269609750	0.695681875
		0.4					1.263454546	0.696754016
			0.4				1.284129154	0.694625358
			0.5				1.310469331	0.691509307
			0.6				1.336358259	0.688464147
				0.4			1.215680214	0.708528391
				0.5			1.174962411	0.718205586
				0.6			1.135020179	0.727071396
					0.2		1.318569570	0.728369261
					0.3		1.382555749	0.760370895
					0.4		1.449242783	0.793811109
						0.2	1.252695434	0.635160040
						0.3	1.247594647	0.572843515
						0.4	1.241824365	0.509429097

that stretching ratio ϵ , porosity parameter λ_1 , inertia coefficient F_r , and suction parameter S are the increasing function of $-f''(0)$, whereas β_t, δ , and α_t are inversely related. The stretching ratio, nonlinear convection, mixed convection, and suction parameters are responsible for the enhancing of the Nusselt number. On the other hand, gradually increasing the porosity parameter, inertia coefficient, and thermal conductivity parameter will reduce the heat transfer rate.

5. CONCLUDING REMARKS

In this study, we have dealt with aspects of the aligned magnetic field past a stratified inclined sheet with nonlinear convection and variable thermal conductivity. Initial equations were altered from nonlinear PDEs to non-dimensional ODEs by incorporating similarity transformation. The resulting problem was nu-

merically solved by employing the shooting technique. After that, we obtained all scenarios of the flow. Exhaustive properties of different physical parameters have been examined through graphs and tables. The following observations were made:

- The local coefficient of the skin friction and Nusselt number increases with the magnetic and suction/injection parameter increase.
- The increasing inclined angle increases to the skin friction and the Nusselt number.
- The velocity decreases for the increasing inclined angle of the sheet.
- The local inertia coefficient is responsible for reducing velocity.
- There is an inverse relationship between the aligned magnetic field and the shrinking/stretching sheet.

CONFLICT OF INTEREST

The authors have no conflict of interest regarding this publication.

REFERENCES

1. SHANKAR D.G., RAJU C.S.K., KUMAR M.S., MAKINDE O.D., Cattaneo-Christov heat flux on an MHD 3D free convection Casson fluid flow over a stretching sheet, *Engineering Transactions*, **68**(3): 223–238, 2020, doi: 10.24423/engtrans.1099.20200720.
2. SAKIDIS B.C., Boundary layer behavior on continuous solid surfaces, *AIChE Journal*, **7**(1): 26–28, 1961, doi: 10.1002/aic.690070108.
3. CHINYOKA T., MAKINDE O.D., Numerical analysis of the transient and non-isothermal channel flow of a third-grade fluid with convective cooling, *Engineering Transactions*, **68**(4): 335–351, 2020, doi: 10.24423/engtrans.1182.20200720.
4. HSIAO K.-L., Micropolar nanofluid flow with MHD and viscous dissipation effects towards a stretching sheet with multimedia feature, *International Journal of Heat and Mass Transfer*, **112**: 983–990, 2017, doi: 10.1016/j.ijheatmasstransfer.2017.05.042.
5. HSIAO K.-L., Combined electrical MHD heat transfer thermal extrusion system using Maxwell fluid with radiative and viscous dissipation effects, *Applied Thermal Engineering*, **112**(5): 1281–1289, 2017, doi: 10.1016/j.applthermaleng.2016.08.208.
6. BILAL M., MAZHAR S.Z., RAMZAN M., MEHMOOD Y., Time dependent hydro-magnetic stagnation point flow of a Maxwell nanofluid with melting heat effect and amended Fourier and Fick's laws, *Heat Transfer*, **50**(5): 4417–4434, 2021, doi: 10.1002/htj.22081.
7. MAKINDE O.D., EEGUNJOBI A.S., Entropy analysis of a variable viscosity MHD Couette flow between two concentric pipes with convective cooling, *Engineering Transactions*, **68**(4): 317–334, 2020, doi: 10.24423/EngTrans.1104.20200720.
8. JANG H.K., HONG S.O., LEE S.B., KIM J.M., HWANG W.R., Viscosity measurement of non-Newtonian fluids in pressure-driven flows of general geometries based on energy

- dissipation rate, *Journal of Non-Newtonian Fluid Mechanics*, **274**: 104204, 2019, doi: 10.1016/j.jnnfm.2019.104204.
9. LENCI A., CHIAPPONI L., An experimental setup to investigate non-Newtonian fluid flow in variable aperture channels, *Water*, **12**(5): 1284, 2020, doi: 10.3390/w12051284.
 10. RAJAGOPAL K.R., GUPTA A.S., Wineman A.S. On a boundary layer theory for non-Newtonian fluids, *International Journal of Engineering Science*, **18**(6): 875–883, 1980, doi: 10.1016/0020-7225(80)90035-X.
 11. ELDESOKY I.M., ABDELSALAM S.I., EL-ASKARY W.A., AHMED M.M., Concurrent development of thermal energy with magnetic field on a particle-fluid suspension through a porous conduit, *BioNanoScience*, **9**: 186–202, 2019, doi: 10.1007/s12668-018-0585-5.
 12. ABDELSALAM S.I., BHATTI M.M., New insight into Au NP applications in tumour treatment and cosmetics through wavy annuli at the nanoscale, *Scientific Reports*, **9**: 260, 2019, doi: 10.1038/s41598-018-36459-0.
 13. BHATTI M.M., MARIN M., ZEESHAN A., ELLAHI R., ABDELSALAM S.I., Swimming of motile gyrostactic microorganisms and nanoparticles in blood flow through anisotropically tapered arteries, *Frontiers in Physics*, **8**: 95, 2020, doi: 10.3389/fphy.2020.00095.
 14. BILAL M., URVA Y., Analysis of non-Newtonian fluid flow over fine rotating thin needle for variable viscosity and activation energy, *Archive of Applied Mechanics*, **91**(3): 1079–1095, 2020, doi: 10.1007/s00419-020-01811-2.
 15. ABDELSALAM S.I., BHATTI M.M., Anomalous reactivity of thermo-bio convective nanofluid towards oxytactic microorganisms, *Applied Mathematics and Mechanics, English Edition*, **41**(5): 711–724, 2020, doi: 10.1007/s10483-020-2609-6.
 16. BILAL M., ASHBAR S., Flow and heat transfer analysis of Eyring-Powell fluid over stratified sheet with mixed convection, *Journal of the Egyptian Mathematical Society*, **28**: 40, 2020, doi: 10.1186/s42787-020-00103-6.
 17. ABDELSALAM S.I., VAFAI K., Combined effects of magnetic field and rheological properties on the peristaltic flow of a compressible fluid in a microfluidic channel, *European Journal of Mechanics – B/Fluids*, **65**: 398–411, 2017, doi: 10.1016/j.euromechflu.2017.02.002.
 18. AKBAR N.S., KHAN Z.H., Effect of variable thermal conductivity and thermal radiation with CNTS suspended nanofluid over a stretching sheet with convective slip boundary conditions: Numerical study, *Journal of Molecular Liquids*, **222**: 279–286, 2016, doi: 10.1016/j.molliq.2016.06.102.
 19. RANA S., MEHMOOD R., AKBAR N.S., Mixed convective oblique flow of a Casson fluid with partial slip, internal heating and homogeneous heterogeneous reactions, *Journal of Molecular Liquids*, **222**: 1010–1019, 2016, doi: 10.1016/j.molliq.2016.07.137.
 20. LU D.-C., RAMZAN M., BILAL M., CHUNG J.D., FAROOQ U., A numerical investigation of 3D MHD rotating flow with binary chemical reaction, activation energy and non-Fourier heat flux, *Communication in Theoretical Physics*, **70**(1): 89–96, 2018, doi: 10.1088/0253-6102/70/1/89.
 21. BILAL M., SAGHEER M., HUSSAIN S., On MHD 3D upper convected Maxwell fluid flow with thermophoretic effect using non-linear radiative heat flux, *Canadian Journal of Physics*, **96**(1): 1–10, 2018, doi: 10.1139/cjp-2017-0250.

22. LU D.-C, RAMZAN M., BILAL M., CHUNG J.D., FAROOQ U., Upshot of chemical species and nonlinear thermal radiation on Oldroyd-B nanofluid flow past a bidirectional stretched surface with heat generation/absorption in a porous media, *Communication in Theoretical Physics*, **70**(1): 71–80, 2018, doi: 10.1088/0253-6102/70/1/71.
23. FORCHHEIMER P.H., *Wasserbewegun Durch Boden Zeitschrift des Vereines Deutscher Ingenieure* [in German], **49**: 1736–1749, 1901.
24. IZBASH S.V., *O Filtracii v Kropnozernstom Materiale* [in Russian], Leningrad, USSR 1931.
25. ALSABERY A.I., TAYEBI T., CHAMKHA A.J., HASHIM I., Natural convection of Al_2O_3 – water nanofluid in a non-Darcian wavy porous cavity under the local thermal non-equilibrium condition, *Scientific Reports*, **10**: 18048, 2020, doi: 10.1038/s41598-020-75095-5.
26. RASOOL G., SHAFIQ A., BALEANU D., Consequences of Soret-Dufour effects, thermal radiation, and binary chemical reaction on Darcy-Forchheimer flow of nanofluids, *Symmetry*, **12**(9): 1421, 2020, doi: 10.3390/sym12091421.
27. SADIQ M.A., HAIDER F., HAYAT T., ALSAEDI A., Partial slip in Darcy-Forchheimer carbon nanotubes flow by rotating disk, *International Communications in Heat and Mass Transfer*, **116**: 104641, 2020, doi:10.1016/j.icheatmasstransfer.2020.104641.
28. PAVLOV K.B., Magneto hydrodynamic flow of an incompressible viscous fluid caused by deformation of a plane surface, *Magneto hydrodynamics*, **10**(4): 507–510, 1974, <http://mhd.sal.lv/contents/1974/4/MG.10.4.23.R.html> (or [in Russian], *Magnitnaya Gidrodinamika*, **4**(1): 146–147, 1974).
29. ANDERSSON H.I., MHD flow of a viscoelastic fluid past a stretching surface, *Acta Mechanica*, **95**(1): 227–230, 1992, doi: 10.1007/BF01170814.
30. MABOOD F., IBRAHIM S.M., RASHIDI M.M., SHADLOO M.S., LORENZINI G., Non-uniform heat source/sink and Soret effects on MHD non-Darcian convective flow past a stretching sheet in a micropolar fluid with radiation, *International Journal of Heat and Mass Transfer*, **93**: 674–682, 2016, doi: 10.1016/j.ijheatmasstransfer.2015.10.014.
31. KHAN M.I., NASIR T., HAYAT T., KHAN N.B., ALSAEDI A., Binary chemical reaction with activation energy in rotating flow subject to nonlinear heat flux and heat source/sink, *Journal of Computational Design and Engineering*, **7**(3): 279–286, 2020, doi: 10.1093/jcde/qwaa023.
32. KUMAR K.A., REDDY J.V.R., SUGUNAMMA V., SANDEEP N., MHD flow of chemically reacting Williamson fluid over a curved/flat surface with variable heat source/sink, *International Journal of Fluid Mechanics Research*, **46**(5): 407–425, 2019, doi: 10.1615/InterJFluidMechRes.2018025940.
33. KHAN A.A., BUKHARI S.R., MARIN M., ELLAHI R., Effects of chemical reaction on third grade MHD fluid flow under the influence of heat and mass transfer with variable reactive index, *Heat Transfer Research*, **50**(11): 1061–1080, 2019, doi: 10.1615/HeatTransRes.2018028397.
34. RAMZAN M., BILAL M., CHUNG J.D., Influence of homogeneous heterogeneous reactions on MHD 3D Maxwell fluid flow with Cattaneo-Christov heat flux and convective boundary condition, *Journal of Molecular Liquids*, **230**: 415–422, 2017, doi: 10.1016/j.molliq.2017.01.061.
35. MAJEED A., ZEESHAN A., NOORI F.M., Analysis of chemically reactive species with mixed convection and Darcy-Forchheimer flow under activation energy: a novel application

- for geothermal reservoirs, *Journal of Thermal Analysis and Calorimetry*, **140**: 2357–2367, 2020, doi: 10.1007/s10973-019-08978-z.
36. MAJEED A., ZEESHAN A., NOORI F.M., Numerical study of Darcy-Forchheimer model with activation energy subject to chemically reactive species and momentum slip of order two, *AIP Advances*, **9**(4): 045035, 2019, doi: 10.1063/1.5095546.
37. RAJU C.S.K., SANDEEP N., SULOCHANA C., SUGUNAMMA V., BABU M.J., Radiation, inclined magnetic field and cross-diffusion effects on flow over a stretching surface, *Journal of the Nigerian Mathematical Society*, **34**(2): 169–180, 2015, doi: 10.1016/j.jnms.2015.02.003.
38. SAJID T., SAGHEER M., HUSSAIN S., BILAL M., Darcy-Forchheimer flow of Maxwell nanofluid flow with nonlinear thermal radiation and activation energy, *AIP Advances*, **8**: 035102, 2018, doi: 10.1063/1.5019218.
39. ILIAS M.R., ISMAIL N.S., ABRAJI N.H., RAWI N.A., SHAFIE S., Unsteady aligned MHD boundary layer flow and heat transfer of a magnetic nanofluids past an inclined plate, *International Journal of Mechanical Engineering and Robotics Research*, **9**(2): 197–206, 2020, doi: 10.18178/ijmerr.9.2.197-206.
40. RAMZAN M., BILAL M., KANWAL S., CHUNG J.D., Effects of variable thermal conductivity and non-linear thermal radiation past an Eyring Powell nanofluid flow with chemical reaction, *Communication in Theoretical Physics*, **67**(6): 723–731, 2017, doi: 10.1088/0253-6102/67/6/723.
41. ABEL M.S., TAWADE J.V., NANDEPPANAVAR M.M., MHD flow and heat transfer for the upper-convected Maxwell fluid over a stretching sheet, *Meccanica*, **47**: 385–393, 2012, doi: 10.1007/s11012-011-9448-7.
42. WAINI I., ZAINAL N.A., KHASHI'IE N.S., Aligned magnetic field effects on flow and heat transfer of the upper-convected Maxwell fluid over a stretching/shrinking sheet, *MATEC Web Conf.*, **97**: 01078, 2017, doi: 10.1051/mateconf/20179701078.
43. BHATTACHARYYA K., Effects of heat source/sink on MHD flow and heat transfer over a shrinking sheet with mass suction, *Chemical Engineering Research Bulletin*, **15**(1): 12–17, 2011, doi: 10.3329/ceerb.v15i1.6524.
44. BILAL M., NAZEER M., Numerical analysis for the non-Newtonian flow over stratified stretching/shrinking inclined sheet with the aligned magnetic field and nonlinear convection, *Archive of Applied Mechanics*, **91**: 949–964, 2021, doi: 10.1007/s00419-020-01798-w.

Received July 28, 2020; accepted version July 8, 2021.

Published on Creative Common licence CC BY-SA 4.0

